



# Cationic iridium (III) complexes bearing fluorinated Ar-BIAN ligands: Synthesis, structure, electronic, and electrochemical properties

Sarvarbek Salohiddinov<sup>a,b</sup>, Arumugam Vignesh<sup>a</sup>, Zilong Li<sup>a,b</sup>, Yanping Ma<sup>a,b,\*</sup>, Wen-Hua Sun<sup>a,b,\*</sup>

<sup>a</sup> Key Laboratory of Engineering Plastics and Beijing National Laboratory for Molecular Sciences, Institute of Chemistry, Chinese Academy of Sciences, Beijing 100190, China

<sup>b</sup> CAS Research/Education Center for Excellence in Molecular Sciences and International School, University of Chinese Academy of Sciences, Beijing 100049, China



## ARTICLE INFO

### Article history:

Received 3 March 2021

Revised 8 June 2021

Accepted 20 July 2021

Available online 23 July 2021

### Keywords:

Cationic iridium complexes

Ar-BIAN

density functional theory

cyclic voltammetry

UV-Vis. absorption

## ABSTRACT

Three cationic iridium (III) complexes, [(ppy)<sub>2</sub>Ir(4-FPhBIAN)]PF<sub>6</sub> (**Ir1**), [(ppy)<sub>2</sub>Ir(3,4-F<sub>2</sub>PhBIAN)]PF<sub>6</sub> (**Ir2**), [(ppy)<sub>2</sub>Ir(4-CF<sub>3</sub>PhBIAN)]PF<sub>6</sub> (**Ir3**) were synthesized from 2-phenylpyridine (Hppy) as cyclometalating ligand and N,N'-bis(aryl)acenaphthene as ancillary ligand. All the complexes were characterized by FT-IR, <sup>1</sup>H, <sup>13</sup>C and <sup>19</sup>F NMR spectroscopies, and elemental analysis. The molecular structures of the complexes were determined by X-ray crystallography. These complexes were crystallized as greenish-black needles in the triclinic *P1* space group for complexes **Ir1** and **Ir3**, while **Ir2** was crystallized in the orthorhombic *P2<sub>1</sub>2<sub>1</sub>2<sub>1</sub>* space group. Electrochemical properties were studied by cyclic voltammetry analysis. All the complexes showed quasi-reversible oxidation and reduction peaks, and reversibility increased by scan rate. Electronic properties were studied by UV-visible spectroscopy, and intense absorption band below 300 nm was obtained compared to intense absorption bands between 300 ~ 530 nm. Density functional theory (DFT) calculations were employed to get better understanding of electrochemical properties.

© 2021 Elsevier B.V. All rights reserved.

## 1. Introduction

Late-transition-metal complexes have received much attentions due to their catalytic, photophysical and electrochemical properties. Nowadays, they are used in innumerable applications such as solid-state lighting applications [1-3], photovoltaic devices [4], biosensing and bioimaging [5]. Among the late-transition metal complexes, Ir(III) complexes have attracted more interests as photoluminescence materials due to higher photoluminescent quantum efficiency, longer lifetime, and high ability to tune the emission color as compared to other transition metal complexes [6-8]. Iridium(III) complexes exhibit high quantum yield as a result of mixed singlet and triplet excited states through strong spin-orbital coupling, leading to high phosphorescence efficiency. Photoluminescent iridium complexes usually contain cyclometalating ligand (phenylpyridine, phenylpyrazole, bipyridine, etc.) and ancillary ligands (bipyridine-based, pyrazole-based, imidazole-based, etc.). These variety of ligands allow to design iridium complexes as ionic [6] or neutral [9] species. Throughout last couple of decades cyclometalated cationic iridium(III) complexes [6] have been exten-

sively studied, especially in the form of [Ir(C<sup>^</sup>N)<sub>2</sub>(N<sup>^</sup>N)]<sup>+</sup> (where C<sup>^</sup>N is cyclometalating ligand in form of 2-phenylpyridine and N<sup>^</sup>N is diimine ancillary ligand). The sterically bulky and highly conjugated diimine type of ligand, bis(arylimino)acenaphthene (Ar-BIAN), have been intensively studied and used as catalytic active complexes for olefin polymerization [10,11]. Photophysical properties of Ir(III) complexes with Ar-BIAN ligands bearing electron-donating and electron-withdrawing groups on *para*-position of the phenyl rings were investigated by Zysman-Colman et al. [12]. They reported the Ir(III) complexes containing *para*-methoxy substituted Ar-BIAN ligands show the absorption energy up to 800 nm, which attracts interest to solar energy harvesting applications [13]. They also reported the cationic Ir(III) and Pt(II) complexes with different derivatives of the Ar-BIAN ligands [14,15]. However, there was no report on the Ir(III) complex bearing fluorine substituted Ar-BIAN ancillary ligands. The ligand bearing fluorine atoms and trifluoromethyl groups have significant influences on the photophysical properties such as emission color, photoluminescence quantum yield and etc. of the Ir(III) complexes [24]. According to existed color tuning strategies of iridium complexes, appending strong electron withdrawing groups to ancillary ligand leads to decrease of HOMO-LUMO band gap and consequently results to a shift of emission color toward lower energy region [6,17]. Ac-

\* Corresponding author.

E-mail addresses: [myanping@iccas.ac.cn](mailto:myanping@iccas.ac.cn) (Y. Ma), [whsun@iccas.ac.cn](mailto:whsun@iccas.ac.cn) (W.-H. Sun).

counting to all above-mentioned points, we designed three different fluorinated ancillary Ar-BIAN ligands to obtain light emission in the lower energy region. The intention of this work was to study on the influence of fluorine atoms in terms of photophysical and electrochemical properties of Ir(III) complexes. Herein, we reported the synthesis and characterization of three cationic iridium complexes [(ppy)<sub>2</sub>Ir(4-FPh-BIAN)]PF<sub>6</sub> (complex **Ir1**), [(ppy)<sub>2</sub>Ir(3,4-FPh-BIAN)]PF<sub>6</sub> (complex **Ir2**), and [(ppy)<sub>2</sub>Ir(4-CF<sub>3</sub>Ph-BIAN)]PF<sub>6</sub> (complex **Ir3**) employing 2-(phenyl)pyridine (ppy) as the cyclometalating ligand and corresponding (Ar-BIAN) ligands as the ancillary ligands. The photophysical and electrochemical properties of these complexes were investigated, and obtained results were corroborated with theoretical DFT calculations.

## 2. Experimental section

### 2.1. Materials and methods

Commercially available reagents were used as received. Reactions were carried out under nitrogen atmosphere using standard Schlenk technique. Iridium dimer [(ppy)<sub>2</sub>Ir(μ-Cl)]<sub>2</sub> was prepared according to literature procedure [18]. <sup>1</sup>H and <sup>13</sup>C NMR spectra were recorded on Bruker Fourier 300 and Bruker Avance 400 MHz instruments respectively, at ambient temperature using TMS as an internal standard. <sup>19</sup>F NMR spectra were logged on a Bruker Ascend 500 MHz instrument. Deuterated chloroform (CDCl<sub>3</sub>) and deuterated dichloromethane (CD<sub>2</sub>Cl<sub>2</sub>) were used as a solvent of record. Chemical shifts are given in parts per million (ppm) and coupling constant (*J*) values in Hz. C, H and N elemental analysis were performed on Flash EA 1112 microanalyzer. Infra-Red spectra were recorded on a Perkin Elmer System 2000 FT-IR. UV-Visible absorption spectra were recorded at room temperature using Shimadzu UV-2600 double beam spectrophotometer. Cyclic voltammetry (CV) analysis of complexes (**Ir1-Ir3**) was recorded on electrochemical workstation CHI-660c. Sample solutions for cyclic voltammetry were prepared in CH<sub>3</sub>CN and degassed with CH<sub>3</sub>CN-saturated nitrogen bubbling for about 20 minutes prior to scanning. Tetra(n-butyl)ammoniumhexafluorophosphate [<sup>n</sup>Bu<sub>4</sub>N]PF<sub>6</sub> 0.1 M in CH<sub>3</sub>CN was used as a supporting electrolyte. [<sup>n</sup>Bu<sub>4</sub>N]PF<sub>6</sub> was recrystallized twice with C<sub>2</sub>H<sub>5</sub>OH and dried under reduced pressure prior to use. The Pt electrode, Pt wire, and Ag/AgCl electrode was used working, counter, and reference electrode, respectively. All the potentials were referred to the ferrocene/ferrocenium (Fc/Fc<sup>+</sup>) taken as internal standard. All the voltametric experiments were started and finished at a potential of 0 V and performed toward clockwise direction [18].

### 2.2. Synthesis of bis(arylimino)-acenaphthene (Ar-BIAN) ligands (L1-L3)

All the ligands were prepared according to the Schiff's base reactions of acenaphthylene-1,2-dione (0.91 g, 5 mmol) with substituted anilines (11 mmol) in the presence of catalytic amount of *p*-toluene sulfonic acid in toluene. Reaction mixture was refluxed for 6 hours at 140°C. Dean-Stark apparatus was used in order to remove secondary product (H<sub>2</sub>O) from the reaction environment. After completion of the reaction, the mixture was cooled to room temperature, solvent was removed under vacuum and crude product was recrystallized twice with ethanol.

*N,N'*-bis(4-fluorophenyl)acenaphthene (4-FPh-BIAN) (**L1**): Obtained as a yellow solid. Yield: 1.41 g, 76 %. <sup>1</sup>H NMR (300 MHz, CDCl<sub>3</sub>) δ (ppm): 7.84 (d, *J* = 8.3 Hz, 2H), 7.35 (dd, *J* = 8.3, 7.2 Hz, 2H), 7.18 – 7.09 (m, 4H), 7.09 – 7.00 (m, 4H), 6.90 (d, *J* = 7.2 Hz, 2H). <sup>13</sup>C NMR (100 MHz, CDCl<sub>3</sub>) δ (ppm): 161.90, 161.89, 161.45, 159.04, 147.67, 147.64, 141.94, 131.39, 129.33, 128.41, 127.77, 123.95, 119.87, 119.80, 116.48, 116.25. <sup>19</sup>F NMR (470 MHz, CDCl<sub>3</sub>) δ (ppm):

-119.19. FT-IR (cm<sup>-1</sup>): 3049 (w), 1658 (m), 1633 (m), 1590 (m), 1496 (s), 1487 (s), 1435 (m), 1419 (m), 1358 (m), 1273 (m), 1211 (s), 1203 (s), 1147 (m), 1090 (m), 1042 (m), 1008 (m), 925 (m), 827 (s), 792 (m), 780 (m), 745 (m), 732 (m), 720 (m). Anal. Calcd. For C<sub>24</sub>H<sub>14</sub>F<sub>2</sub>N<sub>2</sub> (368.39): C, 78.25; H, 3.83; N, 7.60%. Found: C, 78.42; H, 3.78; N, 7.64%.

*N,N'*-bis(3,4-difluorophenyl)acenaphthene (3,4-FPh-BIAN) (**L2**): Obtained as a grayish-yellow solid. Yield: 1.27 g, 63 %. <sup>1</sup>H NMR (300 MHz, CDCl<sub>3</sub>) δ (ppm): 8.06 (d, *J* = 8.3 Hz, 2H), 7.56 (dd, *J* = 8.3, 7.3 Hz, 2H), 7.42 – 7.30 (m, 2H), 7.15 – 6.99 (m, 4H), 6.98 – 6.88 (m, 2H). <sup>13</sup>C NMR (100 MHz, CDCl<sub>3</sub>) δ (ppm): 162.22, 162.21, 152.32, 152.19, 149.84, 149.71, 148.99, 148.87, 147.97, 147.93, 147.89, 147.86, 146.56, 146.43, 142.09, 131.47, 129.79, 127.93, 124.12, 118.32, 118.31, 118.14, 118.13, 114.21, 114.18, 114.15, 114.12, 108.15, 107.95. <sup>19</sup>F NMR (470 MHz, CDCl<sub>3</sub>) δ (ppm): -135.45, -143.36. FT-IR (cm<sup>-1</sup>): 3054 (w), 1914 (w), 1670 (m), 1645 (m), 1599 (m), 1505 (w), 1489 (w), 1437 (w), 1412 (m), 1364 (w), 1321 (s), 1276 (m), 1244 (m), 1157 (m), 1125 (m), 1098 (s), 1062 (m), 1013 (m), 925 (m), 847 (m), 843 (m), 830 (m), 783 (m). Anal. Calcd. For C<sub>24</sub>H<sub>12</sub>F<sub>4</sub>N<sub>2</sub>(404.37): C, 71.29; H, 2.99; N, 6.93%. Found: C, 71.46; H, 2.82; N, 6.91%.

*N,N'*-bis(4-(trifluoromethyl)phenyl)acenaphthene (4-CF<sub>3</sub>Ph-BIAN) (**L3**): Obtained as a yellow solid. Yield: 1.60 g, 68 %. <sup>1</sup>H NMR (300 MHz, CDCl<sub>3</sub>) δ (ppm): 7.96 (d, *J* = 8.3 Hz, 1H), 7.75 (d, *J* = 8.3 Hz, 2H), 7.44 (dd, *J* = 8.3, 7.3 Hz, 1H), 7.23 (d, *J* = 8.2 Hz, 2H), 6.86 (d, *J* = 7.2 Hz, 1H). <sup>13</sup>C NMR (100 MHz, CDCl<sub>3</sub>) δ (ppm): 161.45, 154.62, 142.21, 131.50, 129.82, 128.13, 128.07, 127.06, 127.03, 126.99, 126.95, 126.73, 125.86, 124.31, 123.16, 118.51. <sup>19</sup>F NMR (470 MHz, CDCl<sub>3</sub>) δ (ppm): -61.76. FT-IR (cm<sup>-1</sup>): 3054 (w), 1914 (w), 1671 (m), 1645 (m), 1599 (m), 1507 (w), 1489 (w), 1438 (w), 1412 (m), 1364 (w), 1321 (s), 1284 (m), 1276 (m), 1244 (m), 1157 (m), 1124 (m), 1097 (s), 1062 (s), 1022 (m), 1013 (m), 925 (m), 847 (m), 843 (m), 830 (s), 783 (m), 749 (m), 703 (m). Anal. Calcd. For C<sub>26</sub>H<sub>14</sub>F<sub>6</sub>N<sub>2</sub> (468.40): C, 66.67; H, 3.01; N, 5.98%. Found: C, 66.37; H, 2.97; N, 6.05%.

### 2.3. General procedure for the synthesis of [(C<sup>^</sup>N)<sub>2</sub>Ir(N<sup>^</sup>N)]PF<sub>6</sub> complexes

The dichloro-bridged dimeric iridium complex [Ir(ppy)<sub>2</sub>(μ-Cl)]<sub>2</sub> (107.1 mg, 0.1 mmol) and bis(aryl)acenaphthylene-1,2-dimine (**L1-L3**) (0.21 mmol) were dissolved in the mixture of dry CH<sub>2</sub>Cl<sub>2</sub> (8 mL) and CH<sub>3</sub>OH (8 mL), then refluxed at 60°C under inert (N<sub>2</sub>) atmosphere for 2 hours. Afterward, the reaction was cooled to room temperature. Solid ammonium hexafluorophosphate (NH<sub>4</sub>PF<sub>6</sub>) (65.2 mg, 0.4 mmol) was added to the reaction mixture under stirring for 1 h at ambient temperature. After evaporation of the solvent under reduced pressure the crude product was dissolved in dichloromethane and then filtered off to remove the inorganic impurities. Filtrate was recrystallized with hexane. The desired product was obtained as green powder, which was filtered and dried under reduced pressure for 36 h at 80°C. The complexes were recrystallized again in CH<sub>2</sub>Cl<sub>2</sub>/n-Hex by slow evaporation.

*Iridium(III) bis[2-phenylpyridinato-N,2']-N,N*-bis(4-fluorophenylimino)acenaphthene hexafluorophosphate (**Ir1**): Obtained as a greenish-black solid. Yield: (184 mg, 91%). <sup>1</sup>H NMR (300 MHz, CD<sub>2</sub>Cl<sub>2</sub>) δ (ppm): 8.62 – 8.54 (m, 2H), 8.29 (d, *J* = 8.3 Hz, 2H), 7.98 – 7.89 (m, 2H), 7.81 (d, *J* = 8.2 Hz, 2H), 7.59 (t, *J* = 7.9 Hz, 2H), 7.40 – 7.31 (m, 6H), 7.05 (s, 2H), 6.91 – 6.73 (m, 8H), 6.27 – 6.01 (m, 4H). <sup>13</sup>C NMR (100 MHz, CD<sub>2</sub>Cl<sub>2</sub>) δ (ppm): 173.67, 167.97, 163.54, 161.07, 150.37, 148.18, 146.76, 143.43, 140.97, 139.40, 132.22, 132.18, 131.82, 130.66, 129.47, 126.91, 124.89, 124.73, 124.68, 124.36, 123.18, 122.04, 120.13, 116.87, 116.58. <sup>19</sup>F NMR (470 MHz, CD<sub>2</sub>Cl<sub>2</sub>) δ (ppm): -72.46, -73.97, -112.97. FT-IR (cm<sup>-1</sup>): 3662 (w), 3581 (w), 3049 (w), 1976 (w), 1606 (m), 1586 (m), 1559 (m), 1496 (m), 1479 (m), 1417 (m), 1360 (w), 1319 (w),

1289 (m), 1214 (m), 1156 (m), 1133 (m), 1098 (m), 1059 (m), 1033 (m), 1008 (m), 957 (m), 828 (s), 776 (m), 748 (s), 730 (m). Anal. Calcd. For  $C_{46}H_{30}F_8IrN_4P$  (1013.95): C, 54.49; H, 2.98; N, 5.53%. Found: C, 54.24; H, 2.94; N, 5.47%.

**Iridium(III) bis[2-phenylpyridinato- $N,2'$ ]- $N,N$ -bis(4-fluorophenylimino)acenaphthene hexafluorophosphate (**Ir2**):** Obtained as a greenish-black solid. Yield: (155 mg, 74 %).  $^1H$  NMR (300 MHz,  $CD_2Cl_2$ )  $\delta$  (ppm): 8.55 (d,  $J = 6.6$  Hz, 2H), 8.32 (dd,  $J = 8.3$ , 1.8 Hz, 2H), 8.03 – 7.75 (m, 4H), 7.62 (td,  $J = 7.8$ , 2.0 Hz, 2H), 7.41 (dt,  $J = 12.2$ , 5.2 Hz, 6H), 7.05 (s, 1H), 6.88 (td,  $J = 14.2$ , 7.3 Hz, 7H), 6.17 (m, 2H), 5.95 (m, 2H).  $^{13}C$  NMR (100 MHz,  $CD_2Cl_2$ )  $\delta$  (ppm): 174.17, 156.56, 150.36, 147.16, 143.32, 140.96, 139.59, 132.63, 132.23, 131.83, 130.86, 129.58, 126.60, 125.15, 124.76, 124.64, 123.52, 120.17, 117.25, 116.73.  $^{19}F$  NMR (470 MHz,  $CD_2Cl_2$ )  $\delta$  (ppm): -72.47, -73.99, -134.90, -135.24, -137.01, -137.47. FT-IR ( $cm^{-1}$ ): 3662 (w), 3586 (w), 3058 (w), 1978 (w), 1608 (m), 1583 (m), 1507 (m), 1477 (m), 1419 (m), 1292 (m), 1259 (m), 1210 (m), 1163 (m), 1134 (m), 1113 (m), 1059 (m), 1033 (m), 976 (m), 945 (w), 910 (w), 831 (s), 775 (s), 730 (s), 655 (m). Anal. Calcd. For  $C_{46}H_{30}F_{10}IrN_4P$  (1051.95): C, 52.52; H, 2.87; N, 5.33%. Found: C, 52.71; H, 2.80; N, 5.45%.

**Iridium(III) bis[2-phenylpyridinato- $N,2'$ ]- $N,N$ -bis(4-(trifluoromethyl)phenylimino)acenaphthene hexafluorophosphate (**Ir3**):** Obtained as a greenish-black solid. Yield: (189 mg, 85 %).  $^1H$  NMR (300 MHz,  $CD_2Cl_2$ )  $\delta$  (ppm): 8.63 (q,  $J = 3.4$ , 2.1 Hz, 2H), 8.31 (d,  $J = 8.3$  Hz, 2H), 7.96 (tt,  $J = 7.9$ , 1.8 Hz, 2H), 7.80 (d,  $J = 8.4$  Hz, 2H), 7.60 (t,  $J = 7.8$  Hz, 2H), 7.49 – 7.27 (m, 10H), 7.20 (t,  $J = 6.0$  Hz, 2H), 6.78 (tt,  $J = 8.9$ , 6.5 Hz, 4H), 6.22 (d,  $J = 8.3$  Hz, 2H), 6.12 (dq,  $J = 6.5$ , 2.0 Hz, 2H).  $^{13}C$  NMR (100 MHz,  $CD_2Cl_2$ )  $\delta$  (ppm): 173.93, 167.83, 150.60, 147.45, 147.30, 143.31, 139.59, 132.62, 132.22, 131.72, 130.78, 130.44, 130.11, 129.61, 128.04, 127.06, 126.77, 126.64, 125.34, 125.21, 124.64, 124.60, 123.33, 123.13, 122.63, 120.62, 120.17.  $^{19}F$  NMR (470 MHz,  $CD_2Cl_2$ )  $\delta$  (ppm): -62.88, -72.47, -73.98. FT-IR ( $cm^{-1}$ ): 3369 (w), 3047 (w), 2920 (w), 2850 (w), 1606 (m), 1584 (m), 1510 (w), 1479 (m), 1439 (m), 1415 (m), 1319 (m), 1251 (m), 1228 (m), 1166 (m), 1112 (m), 1013 (m), 961 (m), 826 (s), 778 (m), 750 (s), 729 (s). Anal. Calcd. For  $C_{48}H_{30}F_{12}IrN_4P$  (1113.97): C, 51.75; H, 2.71; N, 5.03%. Found: C, 52.01; H, 2.95; N, 5.17%.

## 2.4. X-ray crystallographic studies

Single-crystals of **Ir1–Ir3** for the X-ray diffraction determination were grown by layering hexane into saturated dichloromethane solution of the corresponding iridium complexes at room temperature. Crystal data were collected by using XtaLAB Synergy-R single-crystal diffractometer with mirror-monochromatic Cu-K $\alpha$  radiation ( $\lambda = 1.54184$  Å) at 170 K. Cell parameters were obtained by the global refinement of the positions of all collected reflections. The structures were solved by direct methods and refined by full-matrix least-squares on  $F^2$ . Hydrogen atoms were placed in geometrically idealized positions and constrained to ride on their parent atoms with C–H distances. The structures were solved with the SHELXT [19<sup>a</sup>] structure solution program integrated in Olex2 [19<sup>b</sup>] software, and refined with SHELXL refinement package with least-squares minimization [20]. The free solvents present in the single crystal were removed by using the SQUEEZE option of the crystallographic program PLATON [21].

## 2.5. Computational details

Density functional theory (DFT) calculations were carried out with the Gaussian 09 Revision E.01 [22]. program package. Becke's three-parameter B3LYP exchange-correlation functional was used, together with the 6-31G\* basis set for C, H, N, F atoms and the "double- $\zeta$ " quality LANL2DZ basis set for the Ir atom [23]. Ground

state geometries were optimized without symmetry constraints. All calculations were performed in the presence of the solvent ( $CH_3CN$ ), by using the Solvation Model based on Density (SMD). Molecular orbital diagrams were drawn by using Multiwfn software [24].

## 3. Result and discussion

### 3.1. Concept of ligand design and synthesis

Generally, the ligands consisting fluorine atoms and trifluoromethyl groups have significant effect on the photophysical properties particularly emission wavelength, quantum yield, and full width at half maximum (FWHM) etc., of the Ir(III) complexes [16]. For instance, the introduction of fluorine atoms could help to tune the emission colors by altering the energy levels of the HOMO and LUMO. Besides, this kind of phosphors designed not only exhibit an excellent solubility in commonly used solvents with chemical stability but also show bright emissions in the blue region when electron withdrawing groups introduced to the cyclometalating ligands [17<sup>a</sup>]. Keeping these points in mind and according to colour tuning strategies of iridium complexes [17<sup>b</sup>], we designed fluorinated ancillary Ar-BIAN ligands and their Ir(III) complexes herein to obtain emission in the lower energy region. Synthetic procedure for Ar-BIAN ligands and their corresponding iridium(III) complexes are depicted in Scheme 1. Initially, desired Ar-BIAN ligands (**L1–L3**) were obtained in 63–76 % of yield via toluene-4-sulfonic acid catalyzed condensation of acenaphthenequinone with corresponding anilines in toluene, under nitrogen atmosphere. In order to increase the product yield, Dean-Stark apparatus was used to remove secondary product ( $H_2O$ ) from the reaction environment, maintaining temperature between 135°C ~ 145°C. **L1** and **L3** were isolated as yellow solids while **L2** was obtained as a greyish-yellow solid. Iridium dimer  $[(ppy)_2Ir(\mu-Cl)]_2$  was prepared according to the reported procedure [18]. All the three cationic iridium complexes (**Ir1–Ir3**) were synthesized with 74 ~ 91% of yield through scission of iridium precursor  $[(ppy)_2Ir(\mu-Cl)]_2$  with corresponding Ar-BIAN ligands (**L1–L3**) in equally mixed  $CH_2Cl_2$  and  $CH_3OH$  solvents. Two hour refluxing under nitrogen atmosphere was enough to fulfill the reaction. Iridium complexes were obtained as their hexafluorophosphate salts  $[(ppy)_2Ir(Ar-BIAN)]^+PF_6^-$  after the addition of solid ammonium hexafluorophosphate ( $NH_4PF_6$ ) by stirring for one hour at ambient temperature. All the ancillary ligands and their iridium complexes were determined by  $^1H$ ,  $^{13}C$  and  $^{19}F$  NMR spectroscopies and elemental analysis.

**X-ray Structures.** X-ray diffraction analysis was carried out for all the complexes. Single-crystals were grown by layering hexane into saturated dichloromethane solution for the corresponding iridium complexes at room temperature. Summary of the crystal data and refinement parameters are given in the experimental section (Table 1).

All these complexes are crystallized as greenish-black needles. **Ir1** and **Ir3** are in the triclinic  $P1$  space group while **Ir2** is in the orthorhombic  $P2_12_12_1$  space group. The difference in space groups may be due to the racemic mixture containing one solvate molecule ( $CH_2Cl_2$ ) in the asymmetric unit of **Ir1** and **Ir3** but not in **Ir2**. Their structures are depicted in Figures 1–3.

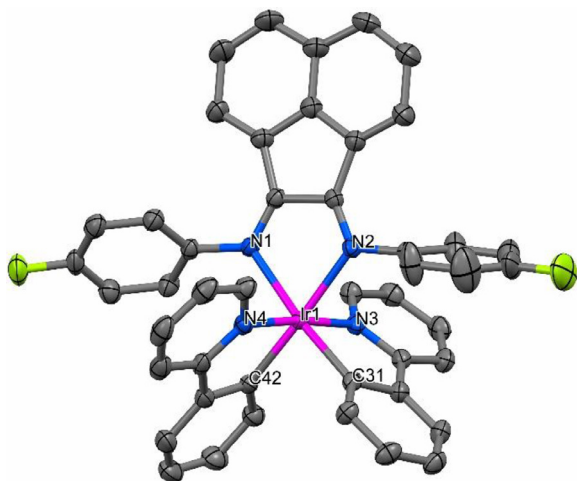
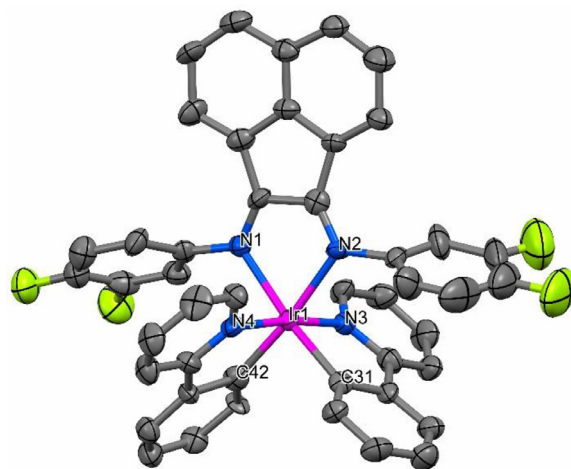
The geometry of all the complexes around the iridium center can be described as disordered-octahedral. Nitrogen atoms of the two coordinated phenylpyridine (ppy) ligands are in a mutually *trans* configuration. The average angles of  $N_{Ar-BIAN}-Ir-N_{Ar-BIAN}$  and  $C_{ppy}-Ir-N_{ppy}$  are 76° and 80° respectively, and the average bond lengths of  $Ir-N_{ppy}$ ,  $Ir-C_{ppy}$  and  $Ir-N_{Ar-BIAN}$  are 2.05 Å, 2.01 Å and 2.17Å, respectively. The selected bond distance and angles are tabulated in Table 2. The torsion of the aryl rings of ancillary (ppy) ligand leads to intramolecular  $\pi$ -stacking interaction with

**Table 1**  
Crystallographic data and refinement parameters for complexes **Ir1–Ir3**.

Compound	Ir1	Ir2	Ir3
CCDC	2065559	2065560	2065561
Empirical formula	IrC <sub>46</sub> H <sub>30</sub> F <sub>2</sub> N <sub>4</sub> PF <sub>6</sub>	IrC <sub>46</sub> H <sub>28</sub> F <sub>4</sub> N <sub>4</sub> PF <sub>6</sub>	IrC <sub>48</sub> H <sub>30</sub> F <sub>6</sub> N <sub>4</sub> PF <sub>6</sub>
Formula weight	1013.95	1049.89	1113.97
Temperature/K	170.01(10)	169.97(10)	169.98(10)
Crystal system, Space group	Triclinic, P-1	Orthorhombic, P2 <sub>1</sub> 2 <sub>1</sub> 2 <sub>1</sub>	Triclinic, P-1
a/Å, α/°	8.71390(10), 99.3090(10)	11.9994(2), 90	12.5303(3), 88.0180(10)
b/Å, β/°	20.7124(3), 99.2110(10)	13.0491(2), 90	14.3972(3), 82.347(2)
c/Å, γ/°	23.5025(2), 96.7840(10)	29.8212(4), 90	25.7647(3), 89.430(2)
Volume/Å <sup>3</sup>	4086.62(9)	4669.44(12)	4603.76(16)
Z; ρ <sub>calc</sub> /cm <sup>3</sup>	2; 1.717	4; 1.493	2; 1.668
μ/mm <sup>-1</sup>	7.967	6.519	7.261
F(000)	2076.0	2056.0	2268.0
Crystal size/mm <sup>3</sup>	0.28 × 0.25 × 0.13	0.55 × 0.23 × 0.06	0.2 × 0.15 × 0.1
Radiation	Cu Kα (λ = 1.54184)	Cu Kα (λ = 1.54184)	Cu Kα (λ = 1.54184)
2θ range for data collection/°	4.372 to 151.012	7.394 to 150.864	6.142 to 151.216
Index ranges	-10 ≤ h ≤ 10, -25 ≤ k ≤ 25, -22 ≤ l ≤ 28	-14 ≤ h ≤ 14, -14 ≤ k ≤ 16, -32 ≤ l ≤ 36	-15 ≤ h ≤ 15, -17 ≤ k ≤ 18, -31 ≤ l ≤ 31
Reflections collected	52846	18959	76428
Independent reflections	16227 [R <sub>int</sub> = 0.0323, R <sub>sigma</sub> = 0.0311]	8721 [R <sub>int</sub> = 0.0501, R <sub>sigma</sub> = 0.0557]	18234 [R <sub>int</sub> = 0.0725, R <sub>sigma</sub> = 0.0569]
Data/restraints/parameters	16227/0/1109	8721/0/560	18234/0/1216
Goodness-of-fit on F <sup>2</sup>	1.053	1.080	1.042
Final R indexes [I > 2σ (I)]	R <sub>1</sub> = 0.0292, wR <sub>2</sub> = 0.0713	R <sub>1</sub> = 0.0452, wR <sub>2</sub> = 0.1192	R <sub>1</sub> = 0.0486, wR <sub>2</sub> = 0.1246
Final R indexes [all data]	R <sub>1</sub> = 0.0342, wR <sub>2</sub> = 0.0745	R <sub>1</sub> = 0.0511, wR <sub>2</sub> = 0.1318	R <sub>1</sub> = 0.0599, wR <sub>2</sub> = 0.1323
Largest diff. peak/hole / e Å <sup>-3</sup>	1.70/-1.03	2.31/-1.17	1.55/-2.18

**Table 2**  
Selected bond lengths and angles.

Complex	Ir1	Ir2	Ir3
bond lengths (Å)			
Ir–C <sub>ppy</sub>	2.009(3), 2.023(3)	1.999(12), 2.045(10)	2.006(5), 2.010(5)
Ir–N <sub>ppy</sub>	2.050(3), 2.051(3)	2.032(8), 2.035(8)	2.050(5), 2.057(5)
Ir–N <sub>Ar-BIAN</sub>	2.172(3), 2.172(3)	2.165(8), 2.174(8)	2.163(4), 2.171(5)
bond angles (°)			
N <sub>ppy</sub> –Ir–C <sub>ppy</sub>	80.25(12), 80.30(13)	79.84(4), 80.64(4)	80.10(2), 80.30(2)
N <sub>Ar-BIAN</sub> –Ir–N <sub>Ar-BIAN</sub>	75.91(10)	75.84(4)	75.62(16)
N <sub>Ar-BIAN</sub> –Ir–C <sub>ppy</sub>	173.12(11), 175.68(11)	171.83(3), 173.04(4)	171.30(2), 172.91(17)
N <sub>ppy</sub> –Ir–N <sub>ppy</sub>	174.64(10)	174.44(4)	174.96(18)

**Figure 1.** Structure of **Ir1**. Thermal ellipsoids are shown at 50% probability level. All the hydrogen atoms, counterion and solvent molecule are omitted for clarity.**Figure 2.** Structure of **Ir2**. Thermal ellipsoids are shown at 50% probability level. All the hydrogen atoms and counterion are omitted for clarity.

the phenyl ring of the cyclometalating (Ar-BIAN) ligands. The average distances between the centroid of these rings are 4.32 Å, 3.94 Å and 4.21 Å for **Ir1**, **Ir2** and **Ir3**, respectively (Figure 4). Additionally, the intramolecular  $\pi$ -stacking makes aryl rings more orthogonal to the acenaphthene core.

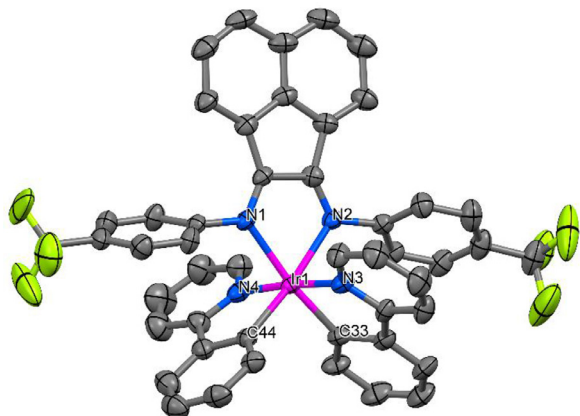
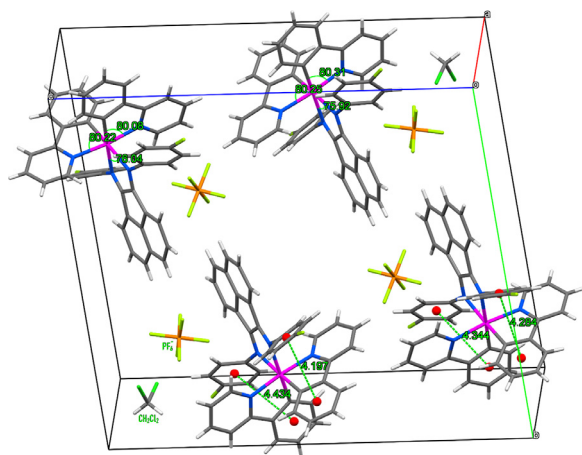
### 3.2. Electrochemical properties

Cyclic voltammetry (CV) analysis of the complexes (**Ir1–Ir3**) was carried out in CH<sub>3</sub>CN solution with 0.1 M [tBu<sub>4</sub>N]PF<sub>6</sub> as the supporting electrolyte. The typical voltammetry cell was composed of

**Table 3**  
Electrochemical data and calculated HOMO and LUMO energies of complexes **Ir1**–**Ir3**.

Complex	Experimental				Calculated		
	$E_{1/2}^{\text{ox}}$ (V) <sup>a</sup>	$E_{1/2}^{\text{red}}$ (V) <sup>a</sup>	$\Delta E_{1/2}$ (V) <sup>b</sup>	$E_{\text{HOMO}}$ (eV) <sup>c</sup>	$E_{\text{HOMO}}$ (eV) <sup>d</sup>	$E_{\text{LUMO}}$ (eV) <sup>d</sup>	$\Delta E$ (eV) <sup>d</sup>
<b>Ir1</b>	+1.33	-0.59	2.00	-5.76	-5.52	-2.88	2.64
<b>Ir2</b>	+1.36	-0.49	1.94	-5.79	-5.54	-2.95	2.59
<b>Ir3</b>	+1.36	-0.47	1.92	-5.80	-5.55	-2.97	2.58

- a)  $E_{1/2}^{\text{ox(red)}} = (E_{\text{pa}} + E_{\text{pc}})/2$   
 b)  $\Delta E_{1/2} = \Delta E_{\text{redox}} = E_{\text{pa}}^{\text{ox}} - E_{\text{pc}}^{\text{red}}$   
 c) Experimentally obtained orbital energies calculated from  $E_{\text{HOMO}} = [-e(E_{\text{onset}}^{\text{ox}} \text{ vs. Ag/AgCl}) - E_{1/2}(\text{Fc/Fc}^+ \text{ vs. Ag/AgCl})] - 4.8$  eV, where  $E_{1/2}(\text{Fc/Fc}^+ \text{ vs. Ag/AgCl})$  is the redox potential of ferrocene in  $\text{CH}_3\text{CN}$  solution, which was found to be 0.41 V [25]  
 d)  $E_{\text{HOMO}}$ ,  $E_{\text{LUMO}}$  and  $\Delta E$  are HOMO, LUMO energies and energy gap obtained from DFT calculations.

**Figure 3.** Structure of **Ir3**. Thermal ellipsoids are shown at 50% probability level. All the hydrogen atoms, counterion and solvent molecule are omitted for clarity.**Figure 4.** Molecular packing diagram of **Ir1** showing intramolecular  $\pi - \pi$  stacking interaction between Aryl and phenyl rings of ligands, distance between their centroids (red balls) in angstrom (Å) and selected bond angles ( $^\circ$ ).

Pt electrode as working electrode, Pt wire as counter electrode, and Ag/AgCl electrode as the reference electrode. The ferrocene ( $\text{Fc/Fc}^+$ ) was used as an internal standard (0.41 V vs. Ag/AgCl) [25]. The electrochemical data obtained at a scan rate of  $50 \text{ mVs}^{-1}$  are summarized in Table 3. The CV traces of all complexes are depicted in Figure 5.

The first oxidation waves (onset) of all the complexes are placed in positive potential region between +1.37 and +1.41 V. This oxidation waves display a bit narrower distribution than reported iridium(III) analogues ( $E^{\text{ox}} = +1.22 \sim +1.60 \text{ V}$ ) [12<sup>a</sup>], and take place on higher potential than the platinum(II) complexes bearing Ar-

BIAN ligands ( $E^{\text{ox}} = +0.85 \sim +1.07 \text{ V}$ ) [15]. For the all cases, the oxidation process is quasi-reversible and peak-to-peak separation values are between 88 ~ 100 mV. As with many cationic iridium complexes [12<sup>a,d</sup>, 13], the oxidation waves correspond to one-electron  $\text{Ir}^{\text{III}}/\text{Ir}^{\text{IV}}$  couple and cyclometalating ppy fragments. The reversible nature of the oxidation is due to major contribution of the iridium 5d orbitals to the highest occupied molecular orbitals (HOMO) compared to ppy ligands. The complexes exhibited better reversibility behavior at the higher scan rate. Figure 5b represents CV voltammogram for **Ir3** with different scan rate. Meanwhile, increasing of the number of fluorine atoms in phenyl rings on the ancillary ligands (from **Ir1** to **Ir2**) leads to slightly shift of oxidation waves toward more positive potentials from +1.37 V to +1.41 V. However, for **Ir2** to **Ir3**, the oxidation onset remains unchanged, equally withdrawing contributions may exist between the *para* -  $\text{CF}_3$  in **Ir3**, *para* and *meta*-F in **Ir2**.

All the three complexes showed quasi-reversible reduction waves in negative potential region from -0.41 V to -0.63 V with a peak-to-peak separation between 68 ~ 78 mV. These reduction waves are cathodically shifted compared to reported iridium(III) complexes (-0.29 ~ -0.57 V) [12<sup>a</sup>]. These peaks show the impact of two fluorine atoms which are directly linked to the phenyl ring ( $E_{\text{onset}}^{\text{red}} = -0.49 \text{ V}$  for **Ir2**) which is nearly as same as influence of the trifluoromethyl group with maximum reduction ( $E_{\text{onset}}^{\text{red}} = -0.47 \text{ V}$  for **Ir3**). However, in comparison with **Ir1**, they are shifted to less negative potential region by introducing more electron withdrawing groups on phenyl rings of the Ar-BIAN ligand in **Ir2** and **Ir3**. The reduction waves are correlated with the lowest unoccupied molecular orbital (LUMO) (Table 3). Thus, the great effect induced by the withdrawing groups in the phenyl rings suggests that the ancillary Ar-BIAN ligands are involved in the LUMOs. HOMO and LUMO orbital energies become more negative (stabilizes) by increasing the influence of fluorine atoms on Ar-BIAN ligands (Figure 5). As far as we know, the increasing of fluorine atoms on the Ar-BIAN ligands causes to decrease both LUMO and HOMO energies because of better stabilization of electrons, which become more attracted to the phenyl fragment. However, energy of LUMO decreases faster than HOMO, from **Ir1** to **Ir3**. The theoretical calculations showed the similar influence of fluorine groups to the HOMO and LUMO energy levels (Figure 7).

### 3.3. Electronic absorption

UV-visible spectra of **Ir1**–**Ir3** were recorded in four different solvents ( $\text{CH}_3\text{CN}$ , EA,  $\text{CH}_2\text{Cl}_2$  and THF) at a concentration of  $1 \times 10^{-5} \text{ M}$  at a 298 K (see supplementary data). Figure 6 depicts UV-vis absorption curves in  $\text{CH}_2\text{Cl}_2$  solution. The absorption band maxima and molar absorptivity data of complexes are collected in Table 4.

The absorption peaks of all three complexes are slightly red shifted compared to their analogues bearing electron donating group on Ar-BIAN ligand. All the complexes displayed intense absorption band below 290 nm. This high intense band relates to

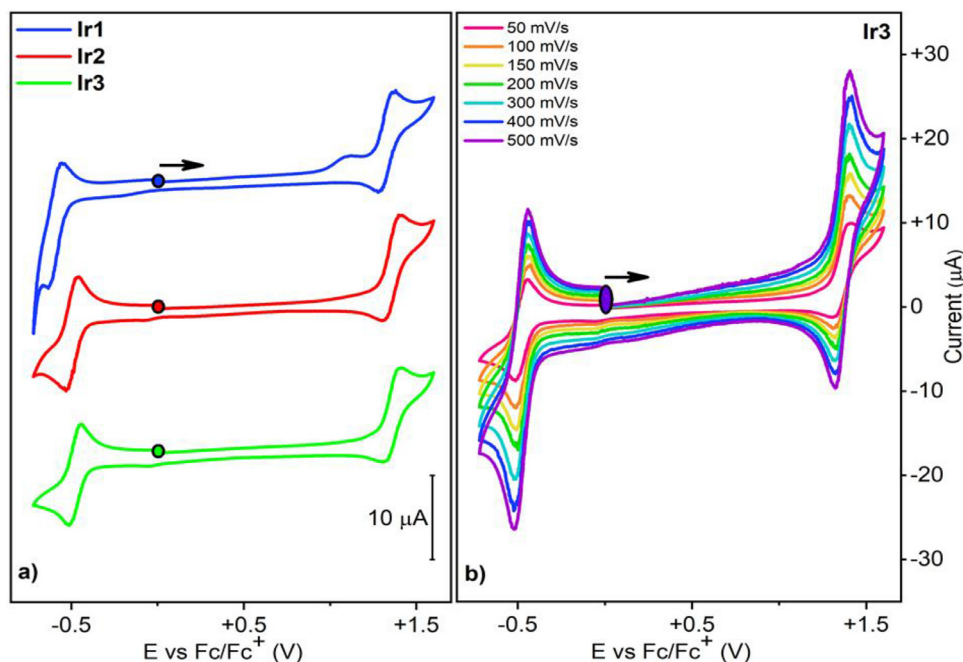


**Figure 5.** (a) Cyclic voltammograms of redox processes of **Ir1–Ir3**, and (b) voltammogram of **Ir3** in different scan rate. The circles refer to starting point and arrow indicates clockwise scanning direction.

**Table 4**  
Absorption data of **Ir1–Ir3**.

Complex	$\lambda_{\text{abs}}/\text{nm}$ ( $\epsilon/\times 10^4 \text{ M}^{-1} \text{ cm}^{-1}$ )
<b>Ir1</b>	254 (5.20), 304 (2.29), 334 (1.93), 412 (1.45), 471 (0.66), 500 (0.02)
<b>Ir2</b>	264 (4.73), 307 (2.14), 354 (1.67), 412 (1.30), 486 (0.53), 500 (0.03)
<b>Ir3</b>	268 (4.72), 307 (2.31), 334 (1.95), 414 (1.18), 487 (0.52), 500 (0.03)

Electronic absorption band ( $\lambda_{\text{abs}}$ ) and molar absorptivity ( $\epsilon$ ) values in  $\text{CH}_2\text{Cl}_2$  at a concentration of  $1 \times 10^{-5} \text{ M}$  at room temperature.

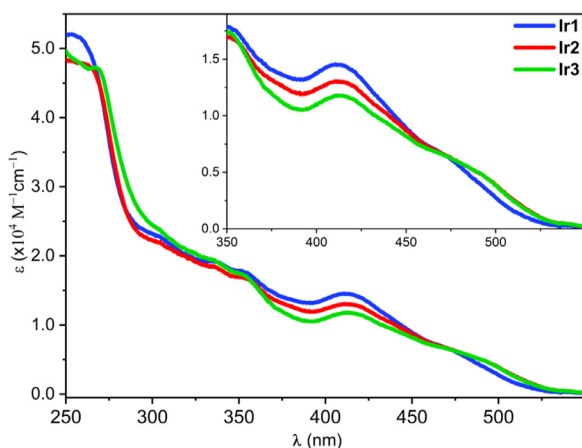


**Figure 6.** UV-Vis absorption plot for **Ir1–Ir3** in  $\text{CH}_2\text{Cl}_2$  solution ( $1.0 \times 10^{-5} \text{ M}$ ), inset is the expansion of 350–550 nm region.

the spin-allowed  $\pi \rightarrow \pi^*$  ligand-centered ( $^1\text{LC}$ ) transitions of the cyclometalating ppy and the ancillary Ar-BIAN ligands [26]. The broad and comparatively less intense absorptions were observed in 290–530 nm range. These low-energy transitions are assigned to the mixed spin-allowed ligand-to-ligand charge transfer ( $^1\text{LLCT}$ ) and metal-to-ligand charge transfer ( $^1\text{MLCT}$ ) [12<sup>a-c</sup>,13]. Absorption curves of all three complexes (**Ir1–Ir3**) are quite similar and does not have significant difference. We believe that the influence of substituted atoms of Ar-BIAN ligands on absorption properties is

not remarkable. The reason for that can be due to quasi-orthogonal orientation of phenyl groups on Ar-BIAN ligand with acenaphthene plane which results to low orbital overlapping with diimine part [27<sup>a</sup>]. For the all three complexes, luminescence analysis was carried out and there was no detectable emission observed. Excitation wavelengths  $\text{Ex}$  were chosen between 290–530 nm. Emission spectra were recorded in  $\text{Ex}+30 \sim 800 \text{ nm}$  range. Samples were prepared among  $1 \times 10^{-4} \sim 1 \times 10^{-5} \text{ M}$  concentration in four different solvents ( $\text{CH}_2\text{Cl}_2$ ,  $\text{CH}_3\text{CN}$ , THF, and EA). All the complexes (**Ir1–Ir3**) are non-emissive, probably due to close lying non-emissive dark state [27<sup>b,c</sup>].

#### 3.4. DFT calculations

In order to gain deep insight into the electrochemical properties of **Ir1–Ir3**, DFT calculations were performed. Geometries of the complexes were optimized by the B3LYP method. The iridium atom was treated with the LANL2DZ basis set, while the other atoms were treated with the 6-31C\* basis set.

The optimized geometries and calculated isodensity surface for HOMOs and LUMOs for all the complexes are in the ground state. The energy diagram from HOMO-4 to LUMO+4 and isodensity surfaces for HOMO and LUMO are depicted in Figure 7. The HOMO of iridium complexes resides on the phenyl  $\pi$ -orbitals of the ppy ligands and  $t_{2g}$  orbitals of the iridium ion, while LUMO locates mostly on acenaphthene plane with small contribution of aryl parts, and LUMO+1 resides only on acenaphthene moiety including nitrogen atoms. The less contribution of aryl rings of the ancillary ligand to

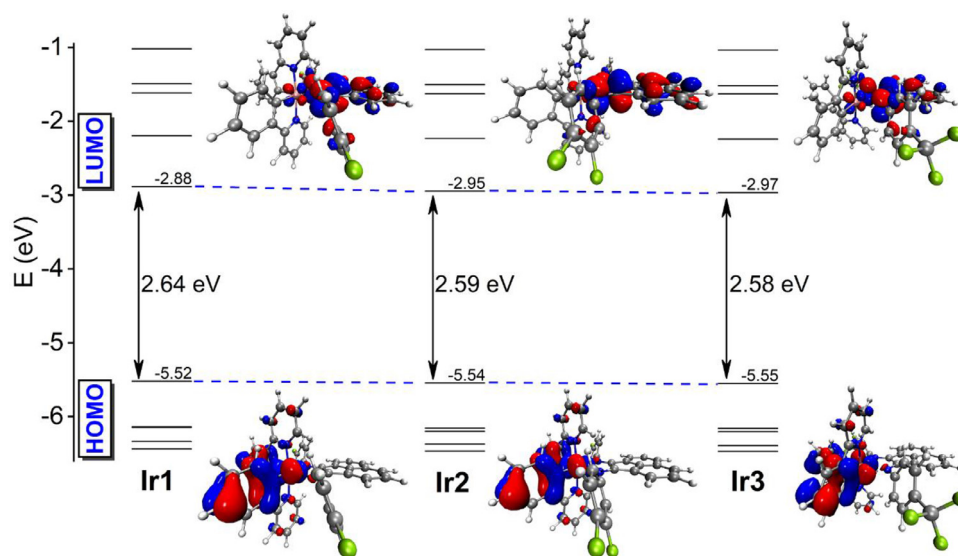
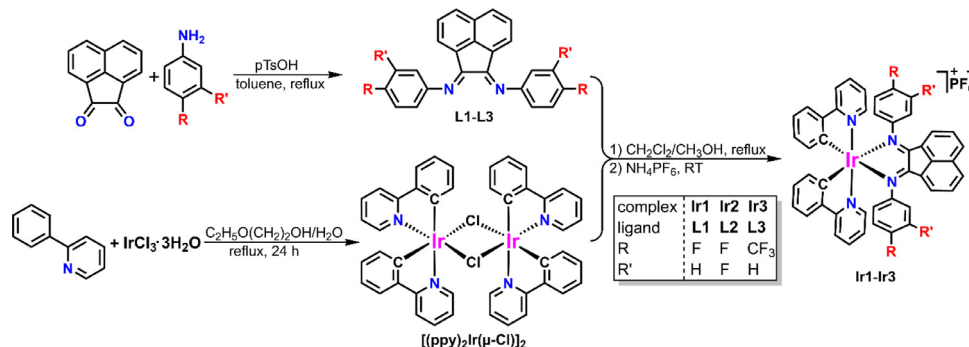


Figure 7. Energy level diagram from HOMO-4 to LUMO+4 and isodensity surface plots for HOMO and LUMO (isovalue = 0.03) of complexes.



Scheme 1. Synthesis of Ar-BIAN ligands and their cationic iridium(III) complexes.

the LUMOs is due to intramolecular  $\pi$ -stacking of the cyclometalating (ppy) and ancillary (Ar-BIAN) ligands. Experimentally obtained HOMO energies decrease from -5.76 eV, -5.79 eV, to -5.80 eV for **Ir1**, **Ir2**, and **Ir3**, while theoretically calculated HOMO energies are from -5.52 eV, -5.54 eV to -5.55 eV, respectively. These obtained values represent good correlation of the experimental and theoretical results. The calculated LUMO energies are -2.88 eV, -2.95 eV and -2.97 eV for **Ir1** to **Ir3**, respectively. The stabilization of LUMOs from **Ir1** to **Ir3** is the result of increasing the number of fluorine atoms on the phenyl ring of Ar-BIAN ligands. Indeed, the impact of fluorine atoms on LUMO energy level is quite low because of the quasi-orthogonal orientation of aryl rings in the acenaphthene plane. However, they still have some contribution in LUMO energy levels. Additionally, increasing the number of electron-withdrawing atoms also leads to slightly stabilization of HOMO energy level. The similar relationship also observed experimentally by cyclic voltammetry analysis. The oxidation and reduction peaks shifted toward more positive potential by increasing the number of fluorine atoms indicating the stabilization of HOMO and LUMO energy levels (Table 3).

#### 4. Conclusion

In this work, three cationic Ir(III) complexes (**Ir1-Ir3**) comprising fluorinated Ar-BIAN ancillary ligands were synthesized and characterized. Molecular structures of all the complexes were determined by the X-ray diffraction analysis. The nitrogen atoms in

ppy ligands were found in mutually *trans* configuration to each other for the all three complexes. All the complexes showed occurrence of intramolecular  $\pi$ -stacking between phenyl part of ppy ligand and aryl parts of Ar-BIAN ligand. However, obvious difference was found between the mono-fluorinated structure and di-fluorinated one. The cyclic voltammetry analysis exhibited that the increasing of fluorine atoms results in shifting of oxidation and reduction peaks to more positive potential which means stabilization of HOMO and LUMO. The same relationship also obtained by DFT calculations. The increase of reversibility of the oxidation traces at higher scan rate shows major contribution of Ir(III) ion compared to ppy ligand, which can be seen from isodensity surface of HOMO. The UV-Vis. absorption curves of the complexes were almost similar for the all three complexes and the effect of fluorine atoms on absorptivity properties was quite low.

#### Declaration of competing interest

The authors declare that they have no known competing financial interests or personal relationships that could have appeared to influence the work reported in this paper.

#### Acknowledgements

This work is supported by the National Natural Science Foundation of China (Nos. 21871275) and the National Key Research and Development Program of China (2016YFB1100801). A.V thanks

the Chinese Academy of Sciences President's International Fellowship Initiative for the award of post-doctoral fellowship (Grant No. 2018PM0012).

## Supplementary materials

Supplementary material associated with this article can be found, in the online version, CCDC numbers 2065559, 2065560 and 2065561 contains the supplementary crystallographic data for the compounds Ir1, Ir2 and Ir3, respectively. Copies of the data can be obtained free of charge via [www.ccdc.cam.ac.uk/data\\_request/cif](http://www.ccdc.cam.ac.uk/data_request/cif) or by emailing [data\\_request@ccdc.cam.ac.uk](mailto:data_request@ccdc.cam.ac.uk) or by contacting the Cambridge Crystallographic Data Center, 12 Union Road, Cambridge CB2 1EZ, UK; phone: +44 (0)1223 336408 fax: +44 (0)1223 336033. at doi:10.1016/j.jorganchem.2021.122002.

## References

- [1] K. Matsuki, J. Pu, T. Takenobu, Recent progress on light-emitting electrochemical cells with nonpolymeric materials, *Adv. Funct. Mater.* 30 (2020) 1908641.
- [2] a) H.C. Su, Y.R. Chen, K.T. Wong, Recent progress in white light-emitting electrochemical cells, *Adv. Funct. Mater.* 30 (2020) 1906898; b) L. Ding, C.X. Zang, L.L. Wen, G.G. Shan, Y. Gao, H.Z. Sun, W.F. Xie, Z.M. Su, High-performance and stable warm white OLEDs based on orange iridium(III) phosphors modified with simple alkyl groups, *Organometallics* 39 (2020) 3384–3393.
- [3] M.Z. Iqbal, S. Alam, M.M. Faisal, S. Khan, Recent advancement in the performance of solar cells by incorporating transition metal dichalcogenides as counter electrode and photoabsorber, *Int. J. Energy Res.* 43 (2019) 3058–3079.
- [4] M.Z. Iqbal, J.U. Nabi, S. Siddique, H.T.A. Awan, S.S. Haider, M. Sulman, Role of graphene and transition metal dichalcogenides as hole transport layer and counter electrode in solar cells, *Int. J. Energy Res.* 44 (2020) 1464–1487.
- [5] a) K.Y. Zhang, Q. Yu, H. Wei, S. Liu, Q. Zhao, W. Huang, Long-lived emissive probes for time-resolved photoluminescence bioimaging and biosensing, *Chem. Rev.* 118 (2018) 1770–1838; b) S.S. Bhat, S. Naveen, V.K. Revankar, N.K. Lokanath, R.V. Pinjari, V. Kumbhar, K. Bhat, Synthesis, structural characterization and biological properties of cyclometalated iridium(III) complexes containing [1,2,5]-thiadiazolo-[3,4-f]-[1,10]-phenanthroline, *New J. Chem.* 44 (2020) 17442–17452.
- [6] R.D. Costa, E. Ortí, H.J. Bolink, F. Monti, G. Accorsi, N. Armaroli, Luminescent ionic transition-metal complexes for light-emitting electrochemical cells, *Angew. Chemie - Int. Ed.* 51 (2012) 8178–8211.
- [7] B. Liu, F. Dang, Z. Feng, Z. Tian, J. Zhao, Y. Wu, X. Yang, G. Zhou, Z. Wu, W.Y. Wong, Novel iridium(III) complexes bearing dimesitylboron groups with nearly 100% phosphorescent quantum yields for highly efficient organic light-emitting diodes, *J. Mater. Chem. C* 5 (2017) 7871–7883.
- [8] a) Y. Jiao, M. Li, N. Wang, T. Lu, L. Zhou, Y. Huang, Z. Lu, D. Luo, X. Pu, A facile color-tuning strategy for constructing a library of Ir(III) complexes with fine-tuned phosphorescence from bluish green to red using a synergetic substituent effect of -OCH<sub>3</sub> and -CN at only the C-ring of C<sup>N</sup> ligand, *J. Mater. Chem. C* 4 (2016) 4269–4277; b) X. Wang, S. Wang, F. Pan, L. He, L. Duan, Cationic iridium complexes with 5-phenyl-1 H-1,2,4-triazole type cyclometalating ligands: toward blue-shifted emission, *Inorg. Chem.* 58 (2019) 12132–12145.
- [9] A.R. Bin Mohd Yusoff, A.J. Huckaba, M.K. Nazeeruddin, Phosphorescent neutral iridium(III) complexes for organic light-emitting diodes, *Top. Curr. Chem. (Z)* 375 (2017) 39.
- [10] a) M.W. Van Laren, C.J. Elsevier, Selective homogeneous palladium(0)-catalyzed hydrogenation of alkynes to (Z)-alkenes, *Angew. Chemie - Int. Ed.* 38 (1999) 3715–3717; b) J. Flapper, J.N.H. Reek, Templated encapsulation of pyridyl-bian palladium complexes: Tunable catalysts for CO/4-tert-butylstyrene copolymerization, *Angew. Chemie - Int. Ed.* 46 (2007) 8590–8592; c) D.H. Leung, J.W. Ziller, Z. Guan, Axial donating ligands: A new strategy for late transition metal olefin polymerization catalysis, *J. Am. Chem. Soc.* 130 (2008) 7538–7539; d) A.E. Cherian, J.M. Rose, E.B. Lobkovsky, G.W. Coates, A C<sub>2</sub>-symmetric, living  $\alpha$ -diimine Ni(II) catalyst: Regioselective copolymers from propylene, *J. Am. Chem. Soc.* 127 (2005) 13770–13771.
- [11] a) H. Liu, W. Zhao, X. Hao, C. Redshaw, W. Huang, W.-H. Sun, 2,6-dibenzhydryl- N -(2-phenyliminoacenaphthylidene)-4- methylbenzenamine nickel dibromides: Synthesis, characterization, and ethylene polymerization, *Organometallics* 30 (2011) 2418–2424; b) D. Jia, W. Zhang, W. Liu, L. Wang, C. Redshaw, W.-H. Sun, Unsymmetrical  $\alpha$ -diiminonickel bromide complexes: Synthesis, characterization and their catalytic behavior toward ethylene, *Catal. Sci. Technol.* 3 (2013) 2737–2745; c) C. Wen, S. Yuan, Q. Shi, E. Yue, D. Liu, W.-H. Sun, Tailoring polyethylenes by nickel complexes bearing modified 1-(2-benzhydrylnaphthylimino)-2-phenyliminoacenaphthylene derivatives, *Organometallics* 33 (2014) 7223–7231; d) S. Yuan, E. Yue, C. Wen, W.-H. Sun, Synthesis, characterization, and ethylene polymerization of 1-[2,4-bis(bis(4-fluorophenyl)methyl)naphthylimino]-2-aryliminoacenaphthylnickel bromides: Influences of polymerization parameters on polyethylenes, *RSC Adv* 6 (2016) 7431–7438; e) X. Wang, L. Fan, Y. Ma, C.Y. Guo, G.A. Solan, Y. Sun, W.-H. Sun, Elastomeric polyethylenes accessible: Via ethylene homo-polymerization using an unsymmetrical  $\alpha$ -diimino-nickel catalyst, *Polym. Chem.* 8 (2017) 2785–2795; f) Z. Wang, Q. Liu, G.A. Solan, W.-H. Sun, Recent advances in Ni-mediated ethylene chain growth: N<sub>imine</sub>-donor ligand effects on catalytic activity, thermal stability and oligo-/polymer structure, *Coord. Chem. Rev.* 350 (2017) 68–83; g) Y. Zeng, Q. Mahmood, Q. Zhang, T. Liang, W.-H. Sun, Highly thermo-stable and electronically controlled palladium precatalysts for vinyl homo/co-polymerization of norbornene-ethylene, *Eur. Polym. J.* 103 (2018) 342–350; h) S.F. Yuan, Z. Fan, Q. Zhang, Z. Flisak, Y. Ma, Y. Sun, W.-H. Sun, Enhancing performance of  $\alpha$ -diiminonickel precatalyst for ethylene polymerization by substitution with the 2,4-bis(4,4'-dimethoxybenzhydryl)-6-methylphenyl group, *Appl. Organomet. Chem.* 34 (2020) 5638–5655.
- [12] a) K. Hasan, E. Zysman-Colman, The effect of aryl substitution on the properties of a series of highly absorptive cationic iridium(III) complexes bearing ancillary bis(arylimino)acenaphthene ligands, *Eur. J. Inorg. Chem.* (2013) 4421–4429; b) T.Y. Li, X. Liang, L. Zhou, C. Wu, S. Zhang, X. Liu, G.Z. Lu, L.S. Xue, Y.X. Zheng, J.L. Zuo, N-heterocyclic carbenes: Versatile second cyclometalated ligands for neutral iridium(III) heteroleptic complexes, *Inorg. Chem.* 54 (2015) 161–173; c) B. Liu, M.A. Javed, J. Guo, W. Xu, S.L. Brown, A. Ugrinov, E.K. Hobbie, S. Kilina, A. Qin, W. Sun, Neutral Cyclometalated Iridium(III) Complexes Bearing Substituted N-Heterocyclic Carbene (NHC) Ligands for High-Performance Yellow OLED Application, *Inorg. Chem.* 58 (2019) 14377–14388; d) A.K. Pal, A.F. Henwood, D.B. Cordes, A.M.Z. Slawin, I.D.W. Samuel, E. Zysman-Colman, Blue-to-Green Emitting Neutral Ir(III) Complexes Bearing Pentafluorosulfanyl Groups: A Combined Experimental and Theoretical Study, *Inorg. Chem.* 56 (2017) 7533–7544.
- [13] K. Hasan, E. Zysman-Colman, Panchromatic cationic iridium(III) complexes, *Inorg. Chem.* 51 (2012) 12560–12564.
- [14] K. Hasan, J. Wang, A.K. Pal, C. Hierlinger, V. Guerschler, H. Sen Soo, F. Garcia, E. Zysman-Colman, Bay-region functionalisation of Ar-BIAN ligands and their use within highly absorptive cationic iridium(III) dyes, *Sci. Rep.* 7 (2017) 15520.
- [15] C. Obrien, M.Y. Wong, D.B. Cordes, A.M.Z. Slawin, E. Zysman-Colman, Cationic platinum(II) complexes bearing Aryl-BIAN ligands: Synthesis and structural and optoelectronic characterization, *Organometallics* 34 (2015) 13–22.
- [16] a) M. Nonoyama, Benzo[h]quinolin-10-yl- N Iridium(III) Complexes, *Bull. Chem. Soc. Jpn.* 47 (1974) 767–768; b) S. Sprouse, K.A. King, P.J. Spellane, R.J. Watts, Photophysical effects of metal-carbon  $\sigma$  bonds in ortho-metallated complexes of Ir(III) and Rh(III), *J. Am. Chem. Soc.* 106 (1984) 6647–6653.
- [17] V.V. Pavlishchuk, A.W. Addison, Conversion constants for redox potentials measured versus different reference electrodes in acetonitrile solutions at 25°C, *Inorganica Chim. Acta.* 298 (2000) 97–102.
- [18] a) G.M. Sheldrick, SHELXT - Integrated space-group and crystal-structure determination, *Acta Crystallogr. Sect. A Found. Crystallogr.* 71 (2015) 3–8; b) L.J. Bourhis, O.V. Dolomanov, R.J. Gildea, J.A.K. Howard, H. Puschmann, The anatomy of a comprehensive constrained, restrained refinement program for the modern computing environment - Olex2 dissected, *Acta Crystallogr. Sect. A Found. Crystallogr.* 71 (2015) 59–75.
- [19] G.M. Sheldrick, Crystal structure refinement with SHELXL, *Acta Crystallogr. Sect. C Struct. Chem.* 71 (2015) 3–8.
- [20] A.L. Spek, PLATON SQUEEZE, A tool for the calculation of the disordered solvent contribution to the calculated structure factors, *Acta Crystallogr. Sect. C Struct. Chem.* 71 (2015) 9–18.
- [21] Gaussian 09, Revision E.01, M. J. Frisch, G. W. Trucks, H. B. Schlegel, G. E. Scuseria, M. A. Robb, J. R. Cheeseman, G. Scalmani, V. Barone, G. A. Petersson, H. Nakatsuji, X. Li, M. Caricato, A. Marenich, J. Bloino, B. G. Janesko, R. Gomperts, B. Mennucci, H. P. Hratchian, J. V. Ortiz, A. F. Izmaylov, J. L. Sonnenberg, D. Williams-Young, F. Ding, F. Lipparini, F. Egidi, J. Goings, B. Peng, A. Petrone, T. Henderson, D. Ranasinghe, V. G. Zakrzewski, J. Gao, N. Rega, G. Zheng, W. Liang, M. Hada, M. Ehara, K. Toyota, R. Fukuda, J. Hasegawa, M. Ishida, T. Nakajima, Y. Honda, O. Kitao, H. Nakai, T. Vreven, K. Throssell, J. A. Montgomery, Jr., J. E. Peralta, F. Ogliaro, M. Bearpark, J. J. Heyd, E. Brothers, K. N. Kudin, V. N. Staroverov, T. Keith, R. Kobayashi, J. Normand, K. Raghavachari, A. Rendell, J. C. Burant, S. S. Iyengar, J. Tomasi, M. Cossi, J. M. Millam, M. Klene, C. Adamo, R. Cammi, J. W. Ochterski, R. L. Martin, K. Morokuma, O. Farkas, J. B. Foresman, and D. J. Fox, Gaussian, Inc., Wallingford CT, 2016.
- [22] a) A.D. Becke, Density-functional thermochemistry. III. The role of exact exchange, *J. Chem. Phys.* 98 (1993) 5648–5652; b) P.J. Hay, W.R. Wadt, Ab initio effective core potentials for molecular calculations. Potentials for K to Au including the outermost core orbitals, *J. Chem. Phys.* 82 (1985) 299–310.
- [23] T. Lu, F. Chen, Multiwfn: A multifunctional wavefunction analyzer, *J. Comput. Chem.* 33 (2012) 580–592.
- [24] P. Tao, W.L. Li, J. Zhang, S. Guo, Q. Zhao, H. Wang, B. Wei, S.J. Liu, X.H. Zhou, Q. Yu, B.S. Xu, W. Huang, Facile Synthesis of Highly Efficient Lepidine-Based Phosphorescent Iridium(III) Complexes for Yellow and White Organic Light-Emitting Diodes, *Adv. Funct. Mater.* 26 (2016) 881–889.
- [25] a) P. Tao, Y. Zhang, J. Wang, L. Wei, H. Li, X. Li, Q. Zhao, X. Zhang, S. Liu, H. Wang, W. Huang, Highly efficient blue phosphorescent iridium(III) complexes with various ancillary ligands for partially solution-processed organic light-emitting diodes, *J. Mater. Chem. C* 5 (2017) 9306–9314; b) A.F. Henwood, E. Zysman-Colman, Lessons learned in tuning the optoelectronic properties of phosphorescent iridium(III) complexes, *Chem. Commun.* 53 (2017) 807–826.
- [26] R.D. Costa, E. Ortí, H.J. Bolink, S. Graber, S. Schaffner, M. Neuberger, C.E. Housecroft, E.C. Constable, Archetype cationic iridium complexes and their use in

- solid-state light-emitting electrochemical cells, *Adv. Funct. Mater.* 19 (2009) 3456–3463.
- [27] a) G. Knör, M. Leirer, T.E. Keyes, J.G. Vos, A. Vogler, Non-luminescent 1,2-diiminetricarbonylrhenium(1) chloride complexes - Synthesis, electrochemical and spectroscopic properties of  $\text{Re}(\text{DIAN})(\text{CO})_2\text{Cl}$  with DIAN = p-substituted bis(arylimino)acenaphthene, *Eur. J. Inorg. Chem.* (2000) 749–751 ;
- b) S. Kammer, I. Starke, A. Pietrucha, A. Kelling, W. Mickler, U. Schilde, C. Dosche, E. Kleinpeter, H.J. Holdt, 1,12-Diazaperylene and 2,11-dialkylated-1,12-diazaperylene iridium(III) complexes  $[\text{Ir}(\text{C}^{\wedge}\text{N})_2(\text{N}^{\wedge}\text{N})]\text{PF}_6$ : New supramolecular assemblies, *Dalt. Trans.* 41 (2012) 10219–10222; c) G. Pourtois, D. Beljonne, C. Moucheron, S. Schumm, A. Kirsch-De Mesmaeker, R. Lazaroni, J.L. Brédas, Photophysical Properties of Ruthenium(II) Polycyclic Aromatic Compounds: A Theoretical Insight, *J. Am. Chem. Soc.* 126 (2004) 683–692.